Force assessment of floating solid particle bed using CFD-DEM modelling

FORCE ASSESSMENT OF FLOATING SOLID PARTICLE BED USING CFD-DEM MODELLING

T.M.J. (Tim) Nijssen, Eindhoven University of Technology
t.m.j.nijssen@tue.nl
K.A. (Kay) Buist, Eindhoven University of Technology
J.A.M. (Hans) Kuipers, Eindhoven University of Technology
J. (Jan) van der Stel, Tata Steel
A.T. (Allert) Adema, Tata Steel

Key Words: Computational Fluid Dynamics (CFD), Discrete Element Method (DEM), Liquid-solid systems, Floating particles, Multiphase flow dynamics.

Abstract

Systems of floating solid particles in liquid are encountered in industry, for example in the ironmaking blast furnace hearth or in slurry bubble columns. Coupled, unresolved CFD-DEM modelling can be used to gain a better understanding of these complex systems. This modelling technique has been applied successfully to gas-solid system by many researchers. In these systems, the particle fluid-interaction is dominated by the drag force. However, when modelling liquid-solid systems, other forces such as lift and virtual mass become of importance. In this work, models are presented for these interaction forces. Finally, a simulation of a floating particle bed in counter-flow is performed. From analysis of the forces, it is shown that at higher Reynolds number (>1000) / high void fraction (>0.7), influence of the lift and virtual mass forces is significant (>10%) and cannot be neglected.

1. INTRODUCTION

Liquid-solid floating particle beds are encountered occasionally in industry, for example in the ironmaking blast furnace hearth [1] or in slurry bubble columns. When modelling such systems, the liquid-solid interaction is often assumed to be dominated by the drag force [2]. However, as the density of the continuous phase is large relative to the particle density, other interaction forces such as the lift force and virtual mass force might contribute to the total interaction force significantly. In this study, unresolved CFD-DEM modelling is used to assess the significance of different liquid-solid interaction forces during flow through a floating particle bed. Previously, CFD-DEM has been applied mainly to gas-solid systems, which can be assumed to be drag-dominated. This work aims towards extending to liquid-solid systems by inclusion of more interaction forces.

2. MODEL DESCRIPTION

In the unresolved CFD-DEM method, fluid flow through the particle bed is resolved only at a length scale larger than the particle, placing its resolution between that of the resolved Euler-Lagrange (immersed boundary) method, and Euler-Euler (two-fluid) models [3]. This allows for the simulation of systems containing interacting fluid and solid phases at a reasonable computational cost [3]. Unresolved CFD-DEM has been applied successfully in numerous systems, such as gas-solid fluidization [4] and geomechanical applications [5]. In this work, the CFDEM®coupling framework [4] is used, which relies on LIGGGHTS® [3] (DEM) and OpenFOAM® (CFD).

a. COMPUTATIONAL FLUID DYNAMICS

Zhou *et al.* [6] reviewed three different model formulations for the continuous phase. One of these, referred to as set II in the work of Zhou or model A in other literature, is used in this work. The (Newtonian and incompressible) fluid flow is governed by the continuity equation (**Equation 1**) and the Navier-Stokes equation (**Equation 2**). Here, $\boldsymbol{f}_{fp}$ represents the total interaction force per unit volume which the fluid exerts on the particles.

b. DISCRETE ELEMENT METHOD

The Discrete Element Method is a well-established method which has been described many times before [7]. The particle trajectories are calculated by integrating Newton's laws of motion using a Velocity Verlet algorithm [8]. In this work, the contact force $\boldsymbol{F}_{pp}$ is given by a Hertzian contact model with a Constant Directional Torque rolling friction model [9]. It should be noted that in unresolved CFD-DEM, the integration timestep for DEM is much smaller (20-500x smaller) than for CFD. The interaction force $\boldsymbol{F}_{fp}$ is evaluated only at the CFD timesteps.

c. INTERACTION FORCES

The total interaction force is the sum of a number of contributions. These interaction forces include the drag, lift, Archimedes, pressure drop, viscous, added mass, Basset and lubrication forces. In the present work, the Basset history and lubrication forces are not taken into account, since their influence is considered small at the scale of the CFD cells. The Archimedes, pressure drop and viscous forces are given by **Equation 9 - 11** respectively.

i. DRAG FORCE

Many drag correlations have been proposed in literature, applicable in different particle Reynolds number ($\mathrm{Re_p} = \rho_f|\boldsymbol{u} - \boldsymbol{v}|d_p/\mu_f$) and solids volume fraction regimes. Most well-know are the work of Stokes [10] (single particle, low $\mathrm{Re_p}$), Turton and Levenspiel [11] (single particle, high $\mathrm{Re_p}$) and Ergun [12] (dense packing, all $\mathrm{Re_p}$). In this work, the drag correlation by Beetstra [13] is used, which was developed for random arrays of spheres at intermediate Reynolds number. The drag force is given by **Equation 3 - 4**.

ii. LIFT FORCE

The lift force is induced by either the vorticity of the fluid field $\boldsymbol{\omega}$ (Saffman lift) or rotation of the particles $\boldsymbol{\Omega}$ (Magnus lift) [14]. McLaughlin [15] and Mei [16] extend the model by Saffman (**Equation 6**, [17]) to finite Reynolds numbers, resulting in **Equation 7**. Loth [18] reported a correlation for the spin-induced lift coefficient at low and intermediate Reynolds numbers ($Re_p < 2000$, **Equation 8**). Since collisions change the particle rotation rapidly, no equilibrium between particle rotation and fluid vorticity can be assumed. Therefore, shear-induced and spin-induced terms are included separately in **Equation 5**.

iii. VIRTUAL MASS FORCE

When a particle accelerates, a part of the fluid around it is accelerated as well, resulting in the virtual mass force. This force is given by **Equation 12**, as formulated by Auton *et al.* [19]. For an isolated particle, $C_{VM,0} = 0.5$ [14]. For groups of particles, a correlation was developed based on the work of Felderhof [20], [21]. **Equation 13 - 14** give the virtual mass coefficient as a function of the solids volume fraction ϵ_s and the specific gravity $\mathrm{SG} = \rho_p/\rho_f$. The coefficients given in **Table 1** were obtained by fitting these equations to the data by Felderhof, as displayed in **Figure 1**. The R^2-value of the fitted curve is 99.6%, indicating a good correspondence. To improve numerical stability, the individual particle velocity $\boldsymbol{v}$ was replaced by the locally averaged solid phase velocity $\boldsymbol{u}_s$. This way, only the acceleration of the particle bulk is considered, not the local acceleration of particles during collisions.

***Table 1**: Coefficients and standard errors for **Equation 13 - 14**.*

i	$a_{i,0}$	$a_{i,1}$
1	0.130 ± 0.0070	0.047 ± 0.0020
2	-0.58 ± 0.041	-0.066 ± 0.0047
3	1.42 ± 0.056	-

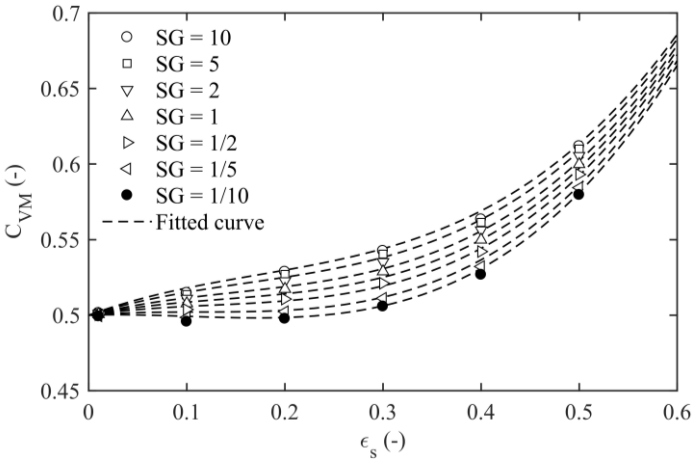

***Figure 1**: Dependency of the virtual mass coefficient on solids volume fraction and specific gravity.*

Fluid motion	
$\frac{\partial \epsilon_f}{\partial t} + \boldsymbol{\nabla} \cdot \left(\epsilon_f \boldsymbol{u}\right) = 0$	**Equation 1**
$\frac{\partial \rho_f \epsilon_f \boldsymbol{u}}{\partial t} + \boldsymbol{\nabla} \cdot \left(\rho_f \epsilon_f \boldsymbol{u}\boldsymbol{u}\right) = -\epsilon_f \boldsymbol{\nabla} p + \epsilon_f \boldsymbol{\nabla} \cdot \left(\mu_f ((\boldsymbol{\nabla u}) + (\boldsymbol{\nabla u})^T)\right) + \rho_f \epsilon_f \boldsymbol{g} - \boldsymbol{f}_{fp}$	**Equation 2**
Drag force	
$\boldsymbol{F}_{drag} = \frac{\pi}{8} d_p^2 \lvert \boldsymbol{u} - \boldsymbol{v} \rvert (\boldsymbol{u} - \boldsymbol{v}) \cdot C_D$	**Equation 3**
$C_D = \frac{24}{\langle \mathrm{Re_p} \rangle} \left[\frac{10(1-\epsilon_f)}{\epsilon_f^2} + \epsilon_f^2 \left(1 + 1.5\sqrt{1-\epsilon_f}\right) \right] + \frac{0.413}{\epsilon_f^2} \left[\frac{\epsilon_f^{-1} + 3\epsilon_f(1-\epsilon_f) + 8.4\langle \mathrm{Re_p} \rangle^{-0.343}}{1 + 10^3 \langle \mathrm{Re_p} \rangle^{-\left(1+4(1-\epsilon_f)\right)/2}} \right]$	**Equation 4**
Lift force	
$\boldsymbol{F}_{Lift} = \frac{\pi}{8} d_p^2 \rho_f \left(C_{L,shear} \lvert \boldsymbol{u} \rvert^2 \frac{\boldsymbol{\omega} \times \boldsymbol{u}}{\lvert \boldsymbol{\omega} \times \boldsymbol{u} \rvert} + C_{L,spin} d_p (\boldsymbol{\Omega} \times \boldsymbol{u}) \right)$	**Equation 5**
$C_{L,Saff} = \frac{12.92}{\pi} \sqrt{\frac{\omega^*}{\mathrm{Re}_p}};\ \ \omega^* = \frac{\lvert \boldsymbol{\omega} \rvert d_p}{\lvert \boldsymbol{u} \rvert}$	**Equation 6**
$C_{L,shear} = 0.3 \left[1 + \tanh\left(\frac{5}{2} \left(\log_{10} \sqrt{\frac{\omega^*}{Re_p}} + 0.191 \right) \right) \right] \cdot \left[\frac{2}{3} + \tanh\left(6 \sqrt{\frac{\omega^*}{Re_p}} - 1.92 \right) \right] \cdot C_{L,Saff}$	**Equation 7**
$C_{L,spin} = 1 - \left[0.675 + 0.15 \left(1 + \tanh\left(0.28(\Omega^* - 2)\right) \right) \right] \cdot \tanh\left(0.18\sqrt{\mathrm{Re_p}}\right);\ \ \Omega^* = \frac{\lvert \boldsymbol{\Omega} \rvert d_p}{\lvert \boldsymbol{u} \rvert}$	**Equation 8**

Other interaction forces		Virtual mass force	
$\boldsymbol{F}_{Arch} = -\rho_f V_p \boldsymbol{g}$	**Equation 9**	$\boldsymbol{F}_{VM} = C_{VM} \rho_f V_p \left(\frac{D\boldsymbol{u}}{Dt} - \frac{d\boldsymbol{u}_s}{dt} \right)$	**Equation 12**
$\boldsymbol{F}_{\nabla p} = (\boldsymbol{\nabla} p) V_p$	**Equation 10**	$C_{VM} = C_{VM,0} + \sum_{i=1}^{3} a_i \epsilon_s^i$	**Equation 13**
$\boldsymbol{F}_{visc} = -(\boldsymbol{\nabla} \cdot \boldsymbol{\tau}) V_p = -\left(\boldsymbol{\nabla} \cdot \left(\mu_f \boldsymbol{\nabla u} \right) \right) V_p$	**Equation 11**	$a_i = a_{i,0} + a_{i,1} \ln(\mathrm{SG})$	**Equation 14**

3. RESULTS AND DISCUSSION

In order to show the significance of the different interaction forces, a CFD-DEM simulation of a floating particle bed in liquid counter-flow inside of a cylindrical periodic channel was performed. **Table 2** lists the simulation parameters. The magnitudes of the different interaction forces (averaged over all particles and time, then normalized by the sum of magnitudes) are displayed in **Figure 2**, both as a function of fluid volume fraction (left) and particle Reynolds number (right). The viscous force is not included in this figure, as its contribution is negligible. Also the Archimedes force is not displayed, as it is constant.

Table 2: *List of simulation parameters.*

Domain		
D_{cyl}	0.25	m
L_{cyl}	0.50	m
ϵ_f	0.5	-
Fluid		
U_0	0.05	m/s
ρ_f	1000	kg/m³
μ_f	10^{-3}	Pa·s
Δt_{CFD}	$5 \cdot 10^{-3}$	s
Δx_{CFD}	0.025	m
Particles		
d_p	0.01	m
ρ_P	500	kg/m³
N_p	$2 \cdot 10^4$	-
E	$5 \cdot 10^6$	Pa
ν_p	0.45	-
e	0.3	-
μ_{fric}	0.5	-
μ_{roll}	0.1	-
Δt_{DEM}	$5 \cdot 10^{-5}$	s

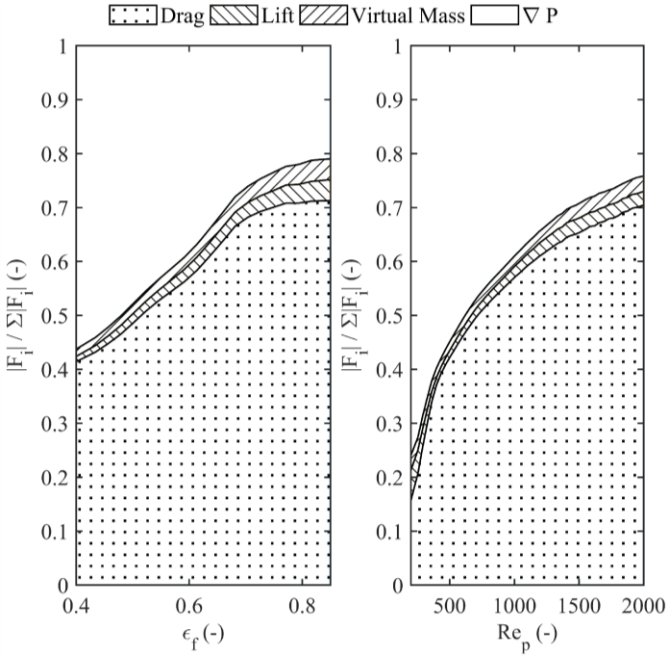

Figure 2*: Relative magnitudes of the interaction forces as a function of void fraction and particle Reynolds number.*

It is clear from **Figure 2** that the drag and pressure drop forces provide the biggest contribution to the total interaction force. However, at higher Reynolds number and/or lower solids fraction the lift and virtual mass force become of increasing importance. Each of their contributions reaches up to 5% of the total interaction force on average, or 10% of the total in instantaneous measurements. This means that these forces cannot be simply neglected for systems of floating particles, as they influence liquid-particle interaction significantly.

4. CONCLUSIONS AND OUTLOOK

In this short paper, the different fluid-particle interaction forces for a system of floating particles in a liquid were assessed. For each force, a model was provided and implement in the CFDEM®coupling framework. A simulation of a floating particle bed in liquid counter-flow was performed. The relative contribution of each of the interaction forces to the total interaction force was analysed and it was found that at higher Reynolds number (>1000) / high void fraction (>0.7), influence of the lift and virtual mass forces is significant (>10%) and cannot be neglected.

In future work, the fluid-particle interaction forces at the particle collision scale (virtual mass, Basset and lubrication forces) will be investigated and implemented in the CFD-DEM model. Together with the large-scale force expressions presented here, these models provide a complete description of the solid-liquid interaction.

This research was carried out under project number s16046 in the framework of the Partnership Program of the Materials innovation institute M2i (www.m2i.nl) and the Technology Foundation STW (www.stw.nl), which is part of the Netherlands Organisation for Scientific Research (www.nwo.nl).

5. REFERENCES

[1] J. G. Peacy and W. G. Davenport, *The Iron Blast Furnace: Theory and Practice*, 1st ed. London: Pergamon Press, 1979.
[2] M. Vångö, S. Pirker, and T. Lichtenegger, "Unresolved CFD–DEM modeling of multiphase flow in densely packed particle beds," *Appl. Math. Model.*, vol. 56, pp. 501–516, 2018.
[3] C. Kloss, C. Goniva, A. Hager, S. Amberger, and S. Pirker, "Models, algorithms and validation for opensource DEM and CFD-DEM," *Prog. Comput. Fluid Dyn. An Int. J.*, vol. 12, no. 2/3, p. 140, 2012.
[4] C. Goniva, C. Kloss, N. G. Deen, J. A. M. Kuipers, and S. Pirker, "Influence of rolling friction on single spout fluidized bed simulation," *Particuology*, vol. 10, no. 5, pp. 582–591, 2012.
[5] J. Zhao and T. Shan, "Coupled CFD-DEM simulation of fluid-particle interaction in geomechanics," *Powder Technol.*, vol. 239, pp. 248–258, 2013.
[6] Z. Y. Zhou, S. B. Kuang, K. W. Chu, and A. B. Yu, "Discrete particle simulation of particle–fluid flow: model formulations and their applicability," *J. Fluid Mech.*, vol. 661, pp. 482–510, 2010.
[7] P. A. Cundall and O. D. L. Strack, "A discrete numerical model for granular assemblies," *Geotechnique*, vol. 1, no. 29, pp. 47–65, 1979.
[8] W. C. Swope, H. C. Andersen, P. H. Berens, and K. R. Wilson, "A computer simulation method for the calculation of equilibrium constants for the formation of physical clusters of molecules: Application to small water clusters," *J. Chem. Phys.*, vol. 76, no. 1, pp. 637–649, 1982.
[9] J. Ai, J. F. Chen, J. M. Rotter, and J. Y. Ooi, "Assessment of rolling resistance models in discrete element simulations," *Powder Technol.*, vol. 206, no. 3, pp. 269–282, 2011.
[10] R. B. Bird, W. E. Stewart, and E. N. Lightfoot, *Transport Phenomena*, 2nd ed. John Wiley and Sons, 2006.
[11] R. Turton and O. Levenspiel, "A short note on the drag correlation for spheres," *Powder Technol.*, vol. 47, no. 1, pp. 83–86, 1986.
[12] S. Ergun and A. A. Orning, "Fluid Flow through Randomly Packed Columns and Fluidized Beds," *Ind. Eng. Chem.*, vol. 41, no. 6, pp. 1179–1184, 1949.
[13] R. Beetstra, M. A. Van Der Hoef, and J. A. M. Kuipers, "Drag Force of Intermediate Reynolds Number Flow Past Mono- and Bidisperse Arrays of Spheres," vol. 53, no. 2, pp. 489–501, 2007.
[14] C. T. Crowe, J. D. Schwarzkopf, M. Sommerfeld, and Y. Tsuji, *Multiphase Flows with Droplets and Particles*, 2nd ed. Boca Raton, FL: CRC Press, 2012.
[15] J. B. McLaughlin, "Inertial migration of a small sphere in linear shear flows," *J. Fluid Mech.*, vol. 224, no. 1, p. 261, 1991.
[16] R. Mei, "An approximate expression for the shear lift force on a spherical particle at finite reynolds number," *Int. J. Multiph. Flow*, vol. 18, no. 1, pp. 145–147, 1992.
[17] P. G. Saffman, "The lift on a small sphere in a slow shear flow," *Fluid Mech.*, vol. 22, pp. 385–400, 1965.
[18] E. Loth, "Lift of a Spherical Particle Subject to Vorticity and/or Spin," *AIAA J.*, vol. 46, no. 4, pp. 801–809, 2008.
[19] T. R. Auton, J. C. R. Hunt, and M. Prud'Homme, "The force exerted on a body in inviscid unsteady non-uniform rotational flow," *J. Fluid Mech.*, vol. 197, no. 1, p. 241, 1988.
[20] B. U. Felderhof, "Virtual mass and drag in two-phase flow," *J. Fluid Mech.*, vol. 225, no. 1, p. 177, 1991.
[21] B. U. Felderhof, "Bounds for the effective dielectric constant of a suspension of uniform spheres," *J. Phys. C Solid State Phys.*, vol. 15, no. 18, pp. 3953–3966, 1982.